Decay-Accelerating Factor suppresses Complement C3 activation and retards Atherosclerosis in Low Density Lipoprotein Receptor Deficient Mice

Short title: DAF protects from atherosclerosis

Viola WY Leung [1, 2†]

Sheng Yun [1†]

Marina Botto[3]

Justin C Mason [1]

Talat H Malik [3]

Wenchao Song [4]

Danielle Paixao-Cavalcante[3]

Matthew C Pickering [3]

Joseph J Boyle [1,2]

Dorian O Haskard [1*]

Vascular Science Section, National Heart and Lung Institute[1], Division of Investigative Sciences[2] and the Molecular Genetics and Rheumatology Section, Division of Medicine [3], Imperial College London, Hammersmith Hospital, London, UK; University of Pennsylvania, Philadephia, USA [4].† SY and VWYL are joint first authors

* Corresponding author: Professor Dorian O. Haskard, Vascular Science Section, Imperial College, Hammersmith Hospital, Du Cane Road, London W12 0NN, UK;

Tel: +44 (0) 208 383 3064; Email: d.haskard@imperial.ac.uk

This work was funded by the British Heart Foundation. The authors have no conflicts of interest.

Number of Text Pages: 34; Figures: 7; Tables: 1

ABSTRACT

Objective**:** Decay-accelerating factor (CD55) is a membrane protein that regulates complement pathway activity at the level of C3. We tested the hypothesis that DAF plays an essential role in limiting complement activation in the arterial wall and protecting from atherosclerosis.

Methods and Results**:** DAF gene targeted mice (*daf-1*$^{-/-}$) mice were crossed with LDL-receptor deficient (*Ldlr*$^{-/-}$) mice. *Daf-1*$^{-/-}$*Ldlr*$^{-/-}$ mice had more extensive *en face* Sudan IV staining of the thoracoabdominal aorta than *Ldlr*$^{-/-}$ mice, both following a 12-week period of low fat diet (4.66 $\pm$ 0.63 % *vs* 2.85 $\pm$ 0.34 %, mean $\pm$ SEM, $p<0.03$), or a high fat diet (11.82 $\pm$ 0.89 % *vs* *Ldlr*$^{-/-}$ 8.11 $\pm$ 1.04 %, $p<0.03$). Aortic root lesions in *daf-1*$^{-/-}$*Ldlr*$^{-/-}$ mice on a low fat diet showed increased size and complexity. DAF deficiency increased deposition of C3d and C5b-9, indicating the importance of DAF for downstream complement regulation in the arterial wall.

Conclusion**:** The acceleration of lesion development in the absence of DAF provides confirmation of the proinflammatory and proatherosclerotic potential of complement activation in the *Ldlr*$^{-/-}$ mouse model. Since upstream complement activation is potentially protective, this study underlines the importance of DAF in shielding the arterial wall from the atherogenic effects of complement.

INTRODUCTION

Complement, a complex cascade of serine proteases, is well characterised as playing a pivotal role in inflammation, and in bridging innate and adaptive immunity (1). In current understanding, complement is triggered by three proximal cascades, the classical, alternative and mannose-binding lectin pathways, which converge on C3 at the central hub of the system. Cleavage of C3 leads to the generation of down-stream proinflammatory mediators, including the anaphylatoxins C3a and C5a and the membrane attack-complex C5b-9. Whilst the assembly and insertion of C5b-9 into cell membranes may lyse non-nucleated cells, sublytic levels can activate proliferation and/or proinflammatory gene expression (2).

There is increasing interest in dissecting the possible roles of complement in atherosclerosis *in vivo* (3;4). Theoretically, many factors might activate complement in the arterial wall, including immunoglobulins, cholesterol crystals, enzymatically-modified LDL and apoptotic cells (5-12). However enzymatically-modified LDL is likely to be the most abundant stimulus for complement activation in atherosclerosis, and may act via the alternative pathway and also via direct binding of C1q and C-reactive protein (CRP) (8;9;13-15). In addition, the classical and alternative pathways are capable of low grade "tick-over" activity (16;17).

Previous experimental work has focused on the effects of natural or experimental deficiency of individual complement pathway components. Relevant studies are as follows: (i) rabbits with natural deficiency of C6 have been shown to be protected from diet-induced atherosclerosis (18;19); (ii) although C5 deficiency has been found to have no effect on lesion development in high fat diet-fed *ApoE*$^{-/-}$ mice (20), a recent

study has shown protective effects of an anti-C5 antibody in *ApoE*$^{-/-}$ mice deficient in both *Cd59a* and *Cd59b* genes (21); (iii) C3 deficient mice crossed with *Ldlr*$^{-/-}$ single knock-out mice have been found to have increased aortic lipid deposition with impaired lesion development beyond the foam cell stage (22); (iv) crossing Factor B deficient mice with *ApoE*$^{-/-}$*Ldlr*$^{-/-}$ double-knock-outs had no effect, arguing against an important role for the alternative pathway in that model (23); and (v) more recently, we have reported that low fat diet-fed *Ldlr*$^{-/-}$ mice deficient in classical pathway activity through gene-targeting of C1q (*C1qa*$^{-/-}$) show accelerated atherosclerosis with increased lesion complexity (24). The increased lesion size and complexity in low fat diet-fed *C1qa*$^{-/-}$*Ldlr*$^{-/-}$ mice was associated with an increase in lesional apoptotic cells, consistent with previous studies which have demonstrated a direct role for C1q in apoptotic cell clearance, independent of terminal pathway activation (25;26). Recently the role of the lectin pathway has also been shown to have atheroprotective functions in mice (27), in line with the involvement of mannose-binding lectin in apoptotic cell clearance and also with the association of mannose-binding lectin deficiency with accelerated atherosclerosis in humans (28;29).

Complement activity is tightly regulated by a number of fluid-phase and membrane-bound inhibitors, including the two glycosylphosphatidylinositol (GPI)-anchored membrane proteins decay-accelerating factor (DAF, CD55) and protectin (CD59). Whereas CD59 inhibits insertion of C9 into cell membranes and thus the development of C5b-9 membrane attack complexes, DAF binds to C3, thereby accelerating the decay of the two C3 convertases, C3Bb (alternative pathway) and C4b2a (classical and mannose-binding lectin pathways) (30-32). Structurally, DAF is a multidomain protein comprising a proximal serine/threonine-rich region and four complement

control protein (CCP) domains, of which CCP2 and CCP3 dissociate C3Bb and C4b2a oligomers into constituent proteins. The catalytic mechanism of DAF activity is not fully clear, but the crystal structure and substitution mutants identify Bb (Tyr338), DAF-CCP2 (Arg69, Arg96) and DAF-CCP3 (Phe148 Leu171) as key residues (33;34).

The mouse has two DAF genes encoding GPI-anchored and trans-membrane forms respectively, with the former being more representative of human DAF (35). Gene-targeting of the GPI-anchored form has led to the generation of a knock-out strain that is healthy but shows exaggerated inflammation in models of renal, autoimmune and nervous system diseases (36-39). Recently no protection or exacerbation of atherosclerosis was observed after crossing these mice with the *ApoE*$^{-/-}$ strain (40).

Observations that the classical pathway exerts atheroprotective effects without terminal pathway activation suggest the importance of a strong complement regulatory system in the arterial wall (14;24). Consistent with this, we and others have recently published evidence that CD59 deficiency leads to an acceleration of atherosclerosis in *Ldlr*$^{-/-}$ and *ApoE*$^{-/-}$ mouse models, establishing the proatherogenic potential of the terminal complement pathway and highlighting the importance of CD59 in its regulation (21;40;41). We show in this paper that DAF also plays a role in the regulation of atherosclerosis in the *Ldlr*$^{-/-}$ model.

MATERIAL AND METHODS

Reagents: Oil Red O (ceristain grade), dextrin, gelatin, Mayer's Haematoxylin, L-glutamic acid, glycerol, sodium azide, calcium chloride, magnesium sulphate and

sodium phosphate were obtained from Merck Biosciences/BDH, Poole, UK. Buffered formal saline (4% w/w formaldehyde solution) was from Pioneer Research Chemicals, Colchester, Essex. OCT compound was from CellPath, Newtown, Powys, UK. Other reagents were from Sigma-Aldrich, Poole, UK.

Antibodies: Primary antibodies included rat anti-mouse macrophages/monocyte MOMA-2 (Serotec, Oxford, UK), alkaline phosphatase-conjugated mouse anti-alpha actin (clone α1A4) (Sigma-Aldrich, Poole, UK), rat monoclonal anti-mouse DAF (clone MD1, a kind gift from Prof BP Morgan, Cardiff, UK), goat anti-mouse IgM (Abcam, Cambridge, UK), and rabbit anti-C5b-9 (Cat. # 204903, Calbiochem, Merck Biosciences, Darmstadt, Germany). Secondary antibodies were biotinylated goat anti-rabbit IgG (DakoCytomation, Cambridgeshire, UK), biotinylated goat anti-mouse IgG (Dako, Ely, UK). Control antibodies were fluorescein-conjugated goat IgG (Santa Cruz Biotechnology, Inc., Heidelberg, Germany), biotinylated goat IgG (R&D Systems, UK), and anti-NFκB p65, biotin-conjugated anti-GFP, rabbit anti-vitronectin, and polyclonal rabbit anti-clusterin (all from Santa Cruz Biotechnology, Inc., Heidelberg, Germany).

Mice: DAF gene-targeted mice (*daf-1*$^{-/-}$) were generated as described (36). *Ldlr*$^{-/-}$ mice were obtained from Jackson Laboratories (Bar Harbor, Maine, USA). Both *daf-1*$^{-/-}$ and *Ldlr*$^{-/-}$ mice were back-crossed for 10 generations on to the C57BL/6 background prior to intercrossing to form *daf-1*$^{-/-}$*Ldlr*$^{-/-}$ double knockout mice. DAF genotypes were determined by polymerase chain reaction. C3 deficient *Ldlr*$^{-/-}$ (*C3*$^{-/-}$*Ldlr*$^{-/-}$) mice were made by crossing *Ldlr*$^{-/-}$ mice with a C3 gene-targeted strain (42). All mice in the study were female. Animals were housed in a specific pathogen-free environment and studied according to UK Home Office regulations. The experimental groups were

gradually transferred onto low fat or high fat diets at 10 weeks of age, as described (41). All mice were studied at 22 weeks of age.

Lipoprotein, cholesterol and triglyceride analysis: Blood was withdrawn from the inferior vena cava after sacrifice and allowed to clot on ice. Serum was kept at 4^{o}C for up to 24 hours before analysis. Lipoprotein profiles were analyzed on pooled sera by size-exclusion chromatography using a SMART^{TM} micro-FPLC system (Pharmacia, Sweden). Serum total cholesterol and triglycerides were measured enzymatically on each individual mouse using Kit Infinity TR13421/2350-250 and Kit Infinity TR22421/2780-250 respectively (MediMark, Grenoble, France) according to the manufacturer's instructions.

Quantification and immunohistochemistry of atherosclerotic lesions: Mice were killed by exsanguinations under carbon dioxide (CO_2). *En face* staining of thoracoabdominal aorta and quantification of the aortic root lesion area were conducted as described (24;41). Immunohistochemistry was performed by standard procedures on residual sections not required for analysis of lesion size, as described (24;41). Results of immunocytochemistry are presented as a percentage area fraction of the aortic root or as the percentage of lesional cells, as analysed by *Image ProPlus* ^{TM} software above.

Confocal microscopy imaging: Cryosections were incubated with combinations of markers including: Cy3-labelled anti-alpha actin (clone α1A4) (Sigma-Aldrich, Poole, UK); AlexaFluor® 488-conjugated CD31 (Clone MEC13.3; BioLegend Inc., San Diego, USA), AlexaFluor® 568-labelled anti-CD68 (MCA1957A488, Serotec, Oxford, UK); fluorescein-conjugated goat IgG fraction to mouse complement C3 (Cat

555000, MP Biomedicals, Solon, Ohio, USA); biotinylated anti-mouse complement 3d (R&D Systems, Abingdon, UK), fluorescein-streptavidin (Vector Laboratories, Peterborough, UK) and rat anti-mouse DAF (clone MD1) followed by biotinylated polyclonal rabbit anti-rat secondary and development with AlexaFluor® 488- or AlexaFluor® 568-conjugated streptavidin (Invitrogen, Paisley, UK). Nuclei in fluorescence sections were then counterstained with TOPRO-3 before mounting in 80% glycerol 20% PBS. Sections were examined by confocal or by standard fluorescence microscopy (for enumerating % actin-positive cells and fibrous caps). The confocal used was a Zeiss LSM510 Meta using a standard trichannel set up using the Ar 488nm line, the HeNe 543nm line and the HeNe 633nm line, a 1 Airy Unit pinhole (adjusted for light wavelength) and 3 photomultipliers fed via green (505-530nm BP), orange-red (560-615nm BP) and far red (LP638nm) filters. As advised by Zeiss, photomultiplier (PMT) voltages and amplifier offset were adjusted online using fast scan to maximise image clarity without saturation, and gain was left at the manufacturer's default. PMT voltages were typically green emission 600V, orange-red emission 400V, and far red emission 200V.

Collagen content in atherosclerotic lesion: Aortic root sections were stained with 1% Sirius red in saturated picric acid (Picrosirius Red) for an hour, as described We adopted as closely as possible the methods of the laboratories of Libby and Hansson (43). Polarising microscopy was used to view these sections at x4 magnification (Olymus BX50). Images were then captured with Olympus DP50 digital microscopy camera. Thin collagen fibres (green) and thick collagen fibers (orange/red) were measured using NIH open access generic image analysis software Image J (http://rsbweb.nih.gov/ij (24)). Images were first converted into three greyscale

images (red, green and blue). For red and green channels, lesions in each aortic root section were carefully drawn. After intensity thresholding each image, we measured the area fraction of threshold collagen (the relative amount of collagen area to selected lesion area) within each aortic root lesion, and expressed this as a percentage.

ELISA for detection of mouse C3: ELISA plates were coated overnight with goat anti-mouse C3 (2mg/ml; MP Biomedicals, OH, USA), which also reacts with C3b, or with goat anti-mouse C3d (2mg/ml; R&D system, MN, USA). After blocking, the plates were incubated with wild-type, factor I-deficient or trypsin-treated wild-type sera as a source of intact C3, C3b and C3d, respectively. Bound C3 was detected by adding biotinylated goat anti-mouse C3d (50ng/ml) or biotinylated goat anti-mouse C3 (50ng/ml). Plates were incubated with streptavidin-AP conjugated and the reaction visualized by subsequent addition of *p*-nitrophenyl phosphate substrate (Sigma Fast ™, Sigma-Aldrich Co., Gillingham, UK).

C3 immunostaining in renal tissue: Kidney frozen sections from factor-I deficient mice were immunostained with FITC-conjugated goat anti-mouse C3 or biotinylated-goat anti mouse C3d. To confirm the affinity of goat anti-mouse C3d antibody the kidney sections from factor-I deficient mice were treated *in vitro* with sera from mice with combined deficiency of factor H and C3 (as source of mouse factor I) for 30 min at 37ºC and immunostained.

Quantification of C3 and C3d deposition: Aortic roots were stained to quantify expression of both C3 and C3d. Sections for each cohort were immunostained and imaged contemporaneously, and quantified by confocal microscopy (Zeiss

LSM510Meta). Green fluorescence staining was quantified by a minor modification of published methods (44;45). Using Image J (http://rsbweb.nih.gov/ij), the operator split the RGB image file for each section and then measured the intensity in the green channel taking care to restrict analysis to the lesion as a region of interest. Within each atherosclerotic lesion, we first obtained the area fraction for positive staining by measuring the total number of pixels and the fraction of those pixels that were non-zero. Using the histogram function on slides stained with the isotype control, a threshold was set below which fluorescence was deemed non-specific. Then, for the specific positive pixels, we measured the absolute fluorescence intensity (44).

Quantification of C5b-9 deposition: Neoepitopes on C5b-9 were detected with a rabbit polyclonal antibody raised against human C5b-9 (Calbiochem, Merck Biosciences, Beeston, UK) that has previously been used by us and others to detect C5b-9 in mouse tissues (23;39). Aortic root sections were stained with anti-C5b-9 or control IgG, followed by biotinylated goat anti-rabbit IgG and the ABC-peroxidase system (Dako, Ely, UK), using 3,3'-diaminobenzidine tetrahydrochloride (DAB) as substrate. Anti-C5b-9 staining was scored blind on a 0, + (weak), ++ (moderate) and +++ (strong) semi-quantitative scale.

Statistics: Typically values for a given aortic root were the mean of five sections. Unless stated otherwise, data are expressed as mean ± standard error of the mean and were analysed by two-tailed Student's t-test. Statistical significance of all tests was defined as $p<0.05$.

RESULTS

Body weight and serum lipids in *daf-1*$^{-/-}$*Ldr*$^{-/-}$ mice: The characteristics of the study groups are shown in Table I. No major differences were observed between *Ldr*$^{-/-}$ *a*nd *daf-1*$^{-/-}$*Ldr*$^{-/-}$ strains in body weight, total serum cholesterol and triglyceride levels. Furthermore, there were no differences in the lipoprotein profiles of *Ldlr*$^{-/-}$ and *daf-1*$^{-/-}$ *Ldlr*$^{-/-}$ mice (not shown).

Effect of DAF deficiency on lesions in *en face* preparations of thoracoabdominal aortae: Whilst lesions in *en face* preparations of thoracoabdominal aortae were barely detectable at 22 weeks in *Ldlr*$^{-/-}$ mice fed a low fat diet, DAF deficiency led to significant enhancement (*daf-1*$^{-/-}$*Ldlr*$^{-/-}$ 4.66 $\pm$ 0.63 % *versus* *Ldlr*$^{-/-}$ 2.85 $\pm$ 0.34 %, mean $\pm$ SEM, $p<0.03$). A high fat diet increased lesion areas in *Ldlr*$^{-/-}$ mice approximately three-fold, with *daf-1*$^{-/-}$*Ldlr*$^{-/-}$ mice still having significantly larger lesions (*daf-1*$^{-/-}$*Ldlr*$^{-/-}$ 11.82 $\pm$ 0.89 % *versus* *Ldlr*$^{-/-}$ 8.11 $\pm$ 1.04 %, $p<0.03$) (Figure 1).

Effect of DAF deficiency on atherosclerotic lesion area: Increased atherosclerotic lesion formation in *daf-1*$^{-/-}$*Ldlr*$^{-/-}$ mice fed a low fat diet was also evident in the aortic roots, with larger lesions, either when expressed as absolute lesion area (*daf-1*$^{-/-}$*Ldlr*$^{-/-}$ 76.16 $\pm$ 9.53 x $10^3 \mu m^2$ *vs* *Ldlr*$^{-/-}$ 29.42 $\pm$ 3.83 x 10^3. μm^2; $p<0.001$), or as a fraction of the aortic root (*daf-1* $^{-/-}$*Ldlr*$^{-/-}$ 6.72 $\pm$ 1.11 % *vs* *Ldlr*$^{-/-}$ 2.64 $\pm$ 0.35 %; $p < 0.005$) (Figure 2). Following a high fat diet, aortic root lesions in *Ldlr*$^{-/-}$ mice were already so large as to be take up around a third of the available lumen, and differences between *Ldlr*$^{-/-}$ and *daf-1*$^{-/-}$*Ldlr*$^{-/-}$ did not reach statistical significance (lesion area fraction in *daf-1*$^{-/-}$*Ldlr*$^{-/-}$ 27.73 $\pm$ 0.96 % *vs* *Ldlr*$^{-/-}$ 22.44 $\pm$ 2.32 %, $p = 0.051$) (Figure 2).

Histological analysis of aortic root lesions: Aortic root lesions in low fat diet-fed *Ldlr*$^{-/-}$ mice were composed almost entirely of macrophages, as detected by mAb Moma-2, with poorly developed shoulders. In contrast, *DAF*$^{-/-}$*Ldlr*$^{-/-}$ mice fed a low fat diet had lesions that had evolved from fatty streaks (Stary-Class II) to fibrous cap lesions (Stary Class IV), as judged by a significant increase in the alpha actin-positive vascular smooth muscle cells (VSMC) within lesions, well-defined shoulders and lipid cores (Figure 3A-D). Lesions in the aortic roots of *Ldlr*$^{-/-}$ mice are well known to be rupture-resistant, and we did not observe ruptured plaques. Quantification of the lesion percentage taken up by VSMC showed an approximately six-fold increase in *daf-1*$^{-/-}$*Ldlr*$^{-/-}$ mice (6.72 ± 2.18 % in *daf-1*$^{-/-}$*Ldlr*$^{-/-}$ *vs* 0.68 ± 0.01 % in *Ldlr*$^{-/-}$, $p < 0.002$) (Figure 3E). Following a high fat diet, the proportion of macrophages in relation to lesional cells dropped (Figure 3F), whilst the number of alpha-actin positive cells was significantly increased to approximately 15% of cells, with no significant differences between strains. In confirmation of the increased complexity of lesions in *daf-1*$^{-/-}$*Ldlr*$^{-/-}$ mice, we observed increased collagen % area fraction of thin collagen fibres (green Picrosirius Red staining) in the absence of DAF, both after a low fat diet (2.19 ± 0.57 in *daf-1*$^{-/-}$*Ldlr*$^{-/-}$ *vs* 0.38 ± 0.16 in *Ldlr*$^{-/-}$; $p < 0.001$) and after a high fat diet (7.74 ± 1.41 *vs* 1.06 ± 0.37; $p < 0.0001$). Similarly, % area fraction of thick collagen fibres (orange-red Picrosirius Red staining) was also increased (4.42 ± 1.01 *vs* 3.70 ± 0.88 after a low fat diet ($p < 0.001$); 10.99 ± 2.11 *vs* 4.30 ± 1.04 ($p < 0.004$) after a high fat diet). We observed diffuse lesional immunostaining of IgM and IgG, which was similar between strains (not shown).

Distribution of DAF**:** Double immunofluorescence confocal staining of arterial tissue of *Ldlr*$^{-/-}$ mice showed clear expression of DAF by endothelial cells and macrophages, although DAF expression by endothelium over lesions appeared reduced (Figure 4A-D). Furthermore, expression on macrophages appeared stronger on subendothelial macrophages than on macrophages nearer the necrotic core (Figure 4E-H). DAF expression by VSMC was weak-absent (Figure 4I-L). Furthermore, when these double-stained sections were considered together, there was no evidence for DAF expression within the acellular lipid core of lesions. There was also strong DAF staining in the adventitia, but this was not characterised further. No DAF staining was detected in aortic roots of *daf-1*$^{-/-}$*Ldlr*$^{-/-}$ mice, verifying the specificity of the rat anti-mouse DAF mAb MD1 (not shown).

Validation of anti-C3d antibody for use on mouse tissues: Before using the anti-C3d antibody to analyse atherosclerotic lesions, we validated its use for the detection of activated C3 in the mouse. First, the anti-C3d antibody failed to react with native C3 in wild-type plasma using a sandwich ELISA, but reacted with wild-type serum activated by trypsin to generate C3d (Figure 5A). The anti-C3d antibody also failed to detect antigen in Factor I deficient serum, in which all circulating C3 has been shown by western blotting to be C3b, and in which there is a defect in cleaving C3b to iC3b or C3d (Figure 5A) (37). As previously reported (38), Factor I deficient mice have readily detectable mesangial deposition of C3b (Figure 5B). No staining was seen with the anti-C3d antibody (Figure 5C), demonstrating that the anti-C3d antibody does not react with C3 or C3b in tissue. Following incubation of the sections with a source of murine factor I (serum from mice deficient in both C3 and factor H), which triggers the physiological cleavage of C3b to iC3b and C3d, mesangial C3

reactivity became apparent using both the anti-C3 and anti-C3d antibody (Figure 5C,D).

Quantification of C3 and C3d deposition: Staining of sections for C3 showed a diffuse distribution within lesions in both strains, although on the low fat diet the area of staining was slightly greater in DAF deficient mice ($p< 0.03$) (Figure 6A). The intensity of C3 fluorescence staining was increased significantly by the high fat-diet in *Ldlr*$^{-/-}$ mice, and was significantly greater in *daf-1*$^{-/-}$*Ldlr*$^{-/-}$ compared to *Ldlr*$^{-/-}$ mice on either diet (Figure 6B). Applying the anti-C3d antibody to aortic root sections, positive staining was seen diffusely, implying complement activation products in both cellular and acellular regions of the plaques (Figure 6E-J). Consistent with uncontrolled complement activation, quantitative immunofluorescence of C3d confirmed a significant four-fold increase in the area and intensity of staining for C3d in *daf-1*$^{-/-}$*Ldlr*$^{-/-}$ on the low fat diet (% of lesion positive for C3d 42.41 $\pm$ 4.01 % *vs* 10.68 $\pm$ 1.13 %, $p < 0.001$) and this increase was amplified by the high fat diet (70.78 $\pm$ 3.55 % *vs.* 22.05 $\pm$ 6.91 %, $p < 0.001$) (Figure 6C,D). Notably, diet made no difference to lesional C3d in *Ldlr*$^{-/-}$ single knock-outs, testifying to the competence of C3 regulation in these animals (Figure 6C,D). No C3 or C3d staining was seen in lesions of C3 deficient *Ldlr*$^{-/-}$ mice after a low or high fat diet, establishing specificity of staining.

Semi-quantitative analysis of C5b-9 deposition: Activation of the terminal pathway, as judged by deposition of C5b-9, was detected with DAB immunocytochemical staining, and assessed on semi-quantitative scale. As shown in Figure 7, C5b-9

deposition was significantly greater in *daf-1*$^{-/-}$*Ldlr*$^{-/-}$ mice than in *Ldlr*$^{-/-}$, both on a low fat diet ($p < 0.002$) and following a high fat diet ($p < 0.001$).

In summary, therefore, deficiency of DAF significantly enhanced complement activation in *Ldlr*$^{-/-}$ mice, as judged both by C3d and C5b-9 deposition, and this was associated with increased atherosclerotic lesion formation.

DISCUSSION

This study provides the first experimental evidence showing the importance of C3 regulation by DAF in protection from atherosclerosis. Thus, DAF deficiency led to an increase in lipid deposition in the aorta and an acceleration of lesion formation and VSMC content in the aortic root. As in our previous studies with C1q and CD59 deficiencies, these changes were most marked in mice fed a low fat diet (24;41). Taking the three studies together, the data are consistent with a homeostatic role for the classical complement pathway in the arterial wall on a low fat diet, which is overridden by the greater inflammatory milieu caused by high fat feeding.

The results of this study need to be seen alongside the previous failure to observe an effect of DAF deficiency on *ApoE*$^{-/-}$ mice (40). It should be noted that the *Ldlr*$^{-/-}$ and *ApoE*$^{-/-}$ mouse models are not totally interchangeable, with atherosclerosis in *ApoE*$^{-/-}$ being less dependent upon diet (46). This may possibly have obscured seeing differences that in *daf-1*$^{-/-}$*Ldlr*$^{-/-}$ mice were most prominent on the low fat diet. Other factors that may have prevented observing a phenotype in *daf-1*$^{-/-}$*ApoE*$^{-/-}$ mice include confounding effects of ApoE deficiency on macrophage and T lymphocyte function (47;48). A further consideration is that our study of *daf-1*$^{-/-}$*Ldlr*$^{-/-}$ mice was restricted

to female mice to reduce experimental variability. As male *Ldlr*$^{-/-}$ mice tend to have more severe disease (49), we do not yet know whether there are gender differences in the effects we have observed.

A central part of this study has been the validation of the use of an anti-C3d antibody for analysis of C3 activation in mouse tissues. This antibody recognises C3d but not intact C3 or C3b, the latter evident from the lack of staining of C3 or C3b in the glomeruli of Factor I deficient mice. We have not specifically examined reactivity of this antibody with iC3b. However, since this C3d-reactive antibody did not recognise native C3, we used it as a marker of C3 activation. Using this antibody, we found that there was detectable C3 activation in the aortic root lesions of *Ldlr*$^{-/-}$ mice fed a low fat diet, and that this was markedly increased in the absence of DAF. Although DAF is primarily considered a cell surface protein, it is also found in soluble form, and this perhaps accounts for the increase in C3d in acellular as well as cellular regions of *daf-1*$^{-/-}$*Ldlr*$^{-/-}$ lesions (50). Although high fat feeding increased C3 activation in DAF deficient mice, no such effect was seen in *Ldlr*$^{-/-}$ single knock-outs, suggesting that DAF normally provides a robust control of C3 activation in response to hyperlipidaemia. It is worth noting that the intensity of C3 staining also increased with high fat feeding, suggesting a positive feedback loop whereby increased availability of C3 in the inflamed arterial wall (for example via local synthesis (51)) may increase C3 activation in the absence of DAF.

We also found that DAF deficiency leads to an obvious increase in C5b-9 deposition in the aortic root, both on the low fat and high fat diets. We interpret this observation as indicating the central importance of C3 in complement regulation and showing that

increased terminal pathway activation in DAF deficient mice is sufficient to overwhelm the inhibitory capacity of CD59. In general, the phenotype of *daf-1*$^{-/-}$*Ldlr*$^{-/-}$ mice was similar to that which we have previously reported for mice lacking CD59, apart from a greater prominence of VSMC in the aortic root lesions of high fat diet fed mice in the latter (41). The cause for this is not clear, but could relate to the capacity of CD59 to protect VSMC from the established pro-proliferative signalling effects of C5b-9 (2;52). In this respect it is notable that VSMC showed only low level DAF expression, in contrast to a high level of CD59 expression seen previously (41).

The mechanisms responsible for the increase in atherosclerosis in DAF deficient animals are likely at least in part to reflect increased C3 activation, and to include an increase in the recruitment and activation of monocytes via anaphylatoxins (C3a and C5a), and the effects on cell activation and proliferation of C5b-9 (2;53). Clearly an increased recruitment of monocytes could also be expected to amplify inflammation through release of cytokines and other inflammatory mediators, but this has not been investigated further. Although we have failed to demonstrate a reduction in C3 serum in *daf-1*$^{-/-}$*Ldlr*$^{-/-}$ mice (not shown), it is also possible that increased systemic complement activation may play a role. We are not aware of any interaction between DAF and the LDL receptor, but DAF does have other reported actions that might possibly have contributed to the effects we have observed, including acting as a signal transduction receptor on monocytes and T lymphocytes and influencing leukocyte adhesion (54-59).

DAF and CD59 are just two of several regulators of complement activity, and establishing the relative roles in this model of other fluid phase (eg Factor H (60)) and

membrane-bound complement regulators now deserves further study, particularly with respect to their relative importance on different cell types (ie macrophages *vs* VSMC). In this context, it should be noted that there is an additional membrane bound inhibitor of C3 activity in the mouse, designated Complement Receptor 1 (CR1)-related gene y (Crry) (61). In view of the clear non-redundant role of DAF demonstrated by our data, determining the relative contributions of DAF and Crry in arterial homeostasis will be of great interest. Further studies will also be needed delineate the effects of agents found to be protective in other arterial disease models, such as C1 esterase inhibitor (62).

Expression of complement proteins and complement regulators has been well documented in human atherosclerosis, underscoring the importance of understanding the details of complement biology in the arterial wall via analysis of mouse models (63). DAF is not expressed on normal VSMC but can be identified on VSMC as well as macrophages in advanced plaques, and is functionally competent as a complement regulator *ex vivo* (64;65). Furthermore, mRNA transcripts for DAF and other complement regulators appear to be proportionately less in plaques than those for complement pathway proteins (51). This imbalance may be particularly important in allowing complement activation, in view of the limited capacity of the soluble regulator Factor H to penetrate into atherosclerotic lesions (60).

In conclusion, we have presented data showing that DAF plays a central role in the regulation of complement activation in the arterial wall in mice, consistent with the emerging paradigm in which the proximal classical complement pathway has a critical homeostatic protective effect while distal complement activity is atherogenic.

REFERENCES

1. Walport MJ: Complement. First of two parts. N Engl J Med 2001, 344: 1058-1066

2. Niculescu F and Rus H: Mechanisms of signal transduction activated by sublytic assembly of terminal complement complexes on nucleated cells. Immunol Res 2001, 24: 191-199

3. Oksjoki R, Kovanen PT, Meri S, and Pentikainen MO: Function and regulation of the complement system in cardiovascular diseases. Front Biosci 2007, 12: 4696-4708

4. Haskard DO, Boyle JJ, and Mason JC: The role of complement in atherosclerosis. Curr Opin Lipidol 2008, 19: 478-482

5. Hansson GK, Holm J, and Kral JG: Accumulation of IgG and complement factor C3 in human arterial endothelium and atherosclerotic lesions. Acta Pathol Microbiol Immunol Scand [A] 1984, 92: 429-435

6. Vlaicu R, Rus HG, Niculescu F, and Cristea A: Immunoglobulins and complement components in human aortic atherosclerotic intima. Atherosclerosis 1985, 55: 35-50

7. Seifert PS and Kazatchkine MD: Generation of complement anaphylatoxins and C5b-9 by crystalline cholesterol oxidation derivatives depends on hydroxyl group number and position. Mol Immunol 1987, 24: 1303-1308

8. Seifert PS, Hugo F, Tranum-Jensen J, Zahringer U, Muhly M, and Bhakdi S: Isolation and characterization of a complement-activating lipid extracted from human atherosclerotic lesions. J Exp Med 1990, 172: 547-557

9. Bhakdi S, Dorweiler B, Kirchmann R, Torzewski J, Weise E, Tranum-Jensen J, Walev I, and Wieland E: On the pathogenesis of atherosclerosis: enzymatic transformation of human low density lipoprotein to an atherogenic moiety. J Exp Med 1995, 182: 1959-1971

10. Torzewski M, Klouche M, Hock J, Messner M, Dorweiler B, Torzewski J, Gabbert HE, and Bhakdi S: Immunohistochemical demonstration of enzymatically modified human LDL and its colocalization with the terminal complement complex in the early atherosclerotic lesion. Arterioscler Thromb Vasc Biol 1998, 18: 369-378

11. Navratil JS, Watkins SC, Wisnieski JJ, and Ahearn JM: The globular heads of C1q specifically recognize surface blebs of apoptotic vascular endothelial cells. J Immunol 2001, 166: 3231-3239

12. Nauta AJ, Trouw LA, Daha MR, Tijsma O, Nieuwland R, Schwaeble WJ, Gingras AR, Mantovani A, Hack EC, and Roos A: Direct binding of C1q to apoptotic cells and cell blebs induces complement activation. Eur J Immunol 2002, 32: 1726-1736

13. Bhakdi S, Torzewski M, Klouche M, and Hemmes M: Complement and atherogenesis: binding of CRP to degraded, nonoxidized LDL enhances complement activation. Arterioscler Thromb Vasc Biol 1999, 19: 2348-2354

14. Bhakdi S, Torzewski M, Paprotka K, Schmitt S, Barsoom H, Suriyaphol P, Han SR, Lackner KJ, and Husmann M: Possible protective role for C-reactive protein in atherogenesis: complement activation by modified lipoproteins halts before detrimental terminal sequence. Circulation 2004, 109: 1870-1876

15. Biro A, Thielens NM, Cervenak L, Prohaszka Z, Fust G, and Arlaud GJ: Modified low density lipoproteins differentially bind and activate the C1 complex of complement. Mol Immunol 2007, 44: 1169-1177

16. Lachmann PJ and Hughes-Jones NC: Initiation of complement activation. Springer Semin Immunopathol 1984, 7: 143-162

17. Manderson AP, Pickering MC, Botto M, Walport MJ, and Parish CR: Continual low-level activation of the classical complement pathway. J Exp Med 2001, 194: 747-756

18. Geertinger P and Sørensen H: On the reduced atherogenic effect of cholesterol feeding in rabbits with congenital complement (C6) deficiency. Artery 1977, 1: 177-184

19. Schmiedt W, Kinscherf R, Deigner HP, Kamencic H, Nauen O, Kilo J, Oelert H, Metz J, and Bhakdi S: Complement C6 deficiency protects against diet-induced atherosclerosis in rabbits. Arterioscler Thromb Vasc Biol 1998, 18: 1790-1795

20. Patel S, Thelander EM, Hernandez M, Montenegro J, Hassing H, Burton C, Mundt S, Hermanowski-Vosatka A, Wright SD, Chao YS, and Detmers PA: ApoE(-/-) mice develop atherosclerosis in the absence of

complement component C5. Biochem Biophys Res Commun 2001, 286: 164-170

21. Wu G, Hu W, Shahsafaei A, Song W, Dobarro M, Sukhova GK, Bronson RR, Shi GP, Rother RP, Halperin JA, and Qin X: Complement Regulator CD59 Protects Against Atherosclerosis by Restricting the Formation of Complement Membrane Attack Complex. Circ Res 2009, 104:550-558

22. Buono C, Come CE, Witztum JL, Maguire GF, Connelly PW, Carroll M, and Lichtman AH: Influence of C3 deficiency on atherosclerosis. Circulation 2002, 105: 3025-3031

23. Persson L, Boren J, Robertson AK, Wallenius V, Hansson GK, and Pekna M: Lack of complement factor C3, but not factor B, increases hyperlipidemia and atherosclerosis in Apolipoprotein E-/- low-density lipoprotein receptor-/- mice. Arterioscler Thromb Vasc Biol 2004, 24: 1062-1067

24. Bhatia V, Yun S, Leung V, Grimsditch CE, Benson GM, Botto M, Boyle JJ, and Haskard DO: Complement C1q reduces early atherosclerosis in low-density lipoprotein receptor-deficient mice. Am J Pathol 2007, 170: 416-426

25. Taylor PR, Carugati A, Fadok VA, Cook HT, Andrews M, Carroll MC, Savill JS, Henson PM, Botto M, and Walport MC: A hierarchial role for classical pathway complement proteins in the clearance of apoptotic cells in vivo. J Exp Med 2001, 192: 359-366

26. Quartier P, Potter PK, Ehrenstein MR, Walport MJ, and Botto M: Predominant role of IgM-dependent activation of the classical pathway in the clearance of dying cells by murine bone marrow-derived macrophages in vitro. Eur J Immunol 2004, 35: 252-260

27. Matthijsen RA, de Winther MP, Kuipers D, van dM, I, Weber C, Herias MV, Gijbels MJ, and Buurman WA: Macrophage-specific expression of mannose-binding lectin controls atherosclerosis in low-density lipoprotein receptor-deficient mice. Circulation 2009, 119: 2188-2195

28. Madsen HO, Videm V, Svejgaard A, Svennevig JL, and Garred P: Association of mannose-binding-lectin deficiency with severe atherosclerosis. Lancet 1998, 352: 959-960

29. Stuart LM, Takahashi K, Shi L, Savill J, and Ezekowitz RA: Mannose-binding lectin-deficient mice display defective apoptotic cell clearance but no autoimmune phenotype. J Immunol 2005, 174: 3220-3226

30. Lublin DM and Atkinson JP: Decay-accelerating factor: biochemistry, molecular biology, and function. Annu Rev Immunol 1989, 7: 35-58

31. Rollins SA and Sims PJ: The complement-inhibitory activity of CD59 resides in its capacity to block incorporation of C9 into membrane C5b-9. J Immunol 1990, 144: 3478-3483

32. Meri S, Morgan BP, Davies A, Daniels RH, Olavesen MG, Waldmann H, and Lachmann PJ: Human protectin (CD59), an 18,000-20,000 MW complement lysis restricting factor, inhibits C5b-8 catalysed insertion of C9 into lipid bilayers. Immunology 1990, 71: 1-9

33. Uhrinova S, Lin F, Ball G, Bromek K, Uhrin D, Medof ME, and Barlow PN: Solution structure of a functionally active fragment of decay-accelerating factor. Proc Natl Acad Sci U S A 2003, 100: 4718-4723

34. Kuttner-Kondo L, Hourcade DE, Anderson VE, Muqim N, Mitchell L, Soares DC, Barlow PN, and Medof ME: Structure-based mapping of DAF active site residues that accelerate the decay of C3 convertases. J Biol Chem 2007, 282: 18552-18562

35. Spicer AP, Seldin MF, and Gendler SJ: Molecular cloning and chromosomal localization of the mouse decay- accelerating factor genes. Duplicated genes encode glycosylphosphatidylinositol-anchored and transmembrane forms. J Immunol 1995, 155: 3079-3091

36. Sun X, Funk CD, Deng C, Sahu A, Lambris JD, and Song WC: Role of decay-accelerating factor in regulating complement activation on the erythrocyte surface as revealed by gene targeting. Proc Natl Acad Sci U S A 1999, 96: 628-633

37. Sogabe H, Nagaku M, Ishibashi Y, Wada T, Fujita T, Sun X, Miwa T, Madaio MP, and Song W-P: Increased susceptibility of decay-accelerating factor deficient mice to anti-glomerular basement membrane glomerlonephritis. J Immunol 2001, 167: 2791-2797

38. Miwa T, Maldonado MA, Zhou L, Sun X, Luo HY, Cai D, Werth VP, Madaio MP, Eisenberg RA, and Song WC: Deletion of decay-accelerating factor (CD55) exacerbates autoimmune disease development in MRL/lpr mice. Am J Pathol 2002, 161: 1077-1086

39. Morgan BP, Chamberlain-Banoub J, Neal JW, Song W, Mizuno M, and Harris CL: The membrane attack pathway of complement drives pathology in passively induced experimental autoimmune myasthenia gravis in mice. Clin Exp Immunol 2006, 146: 294-302

40. An G, Miwa T, Song WL, Lawson JA, Rader DJ, Zhang Y, and Song WC: CD59 but not DAF deficiency accelerates atherosclerosis in female ApoE knockout mice. Mol Immunol 2009, 46: 1702-1709

41. Yun S, Leung VW, Botto M, Boyle JJ, and Haskard DO: Accelerated Atherosclerosis in Low-Density Lipoprotein Receptor-Deficient Mice Lacking the Membrane-Bound Complement Regulator CD59. Arterioscler Thromb Vasc Biol 2008, 28: 1714-1716

42. Wessels MR, Butko P, Ma M, Warren HB, Lage AL, and Carroll MC: Studies of group B streptococcal infection in mice deficient in complement component C3 or C4 demonstrate an essential role for complement in both innate and acquired immunity. Proc Natl Acad Sci U S A 1995, 92: 11490-11494

43. Ovchinnikova O, Robertson AK, Wagsater D, Folco EJ, Hyry M, Myllyharju J, Eriksson P, Libby P, and Hansson GK: T-cell activation leads to reduced collagen maturation in atherosclerotic plaques of Apoe(-/-) mice. Am J Pathol 2009, 174: 693-700

44. Kinderlerer AR, Ali F, Johns M, Lidington EA, Leung V, Boyle JJ, Hamdulay SS, Evans PC, Haskard DO, and Mason JC: KLF2-dependent, shear stress-induced expression of CD59: a novel cytoprotective mechanism

against complement-mediated injury in the vasculature. J Biol Chem 2008, 283: 14636-14644

45. Rose KL, Paixao-Cavalcante D, Fish J, Manderson AP, Malik TH, Bygrave AE, Lin T, Sacks SH, Walport MJ, Cook HT, Botto M, and Pickering MC: Factor I is required for the development of membranoproliferative glomerulonephritis in factor H-deficient mice. J Clin Invest 2008, 118: 608-618

46. Joven J, Rull A, Ferre N, Escola-Gil JC, Marsillach J, Coll B, onso-Villaverde C, Aragones G, Claria J, and Camps J: The results in rodent models of atherosclerosis are not interchangeable The influence of diet and strain. Atherosclerosis 2007,

47. Pepe MG and Curtiss LK: Apolipoprotein E is a biologically active constituent of the normal immunoregulatory lipoprotein, LDL-In. J Immunol 1986, 136: 3716-3723

48. Grainger DJ, Reckless J, and McKilligin E: Apolipoprotein E modulates clearance of apoptotic bodies in vitro and in vivo, resulting in a systemic proinflammatory state in apolipoprotein E-deficient mice. J Immunol 2004, 173: 6366-6375

49. Johnson RC, Chapman SM, Dong ZM, Ordovas JM, Mayadas TN, Herz J, Hynes RO, Schaefer EJ, and Wagner DD: Absence of P-selectin delays fatty streak formation in mice. J Clin Invest 1997, 99: 1037-1043

50. Miot S, Crespo S, and Schifferli JA: Distinct forms of DAF in urine and blood. J Immunol Methods 2002, 260: 43-53

51. Yasojima K, Schwab C, McGeer EG, and McGeer PL: Complement components, but not complement inhibitors, are upregulated in atherosclerotic plaques. Arterioscler Thromb Vasc Biol 2001, 21: 1214-1219

52. Niculescu F, Badea T, and Rus H: Sublytic C5b-9 induces proliferation of human aortic smooth muscle cells: role of mitogen activated protein kinase and phosphatidylinositol 3-kinase. Atherosclerosis 1999, 142: 47-56

53. Zwirner J, Werfel T, Wilken HC, Theile E, and Gotze O: Anaphylatoxin C3a but not C3a(desArg) is a chemotaxin for the mouse macrophage cell line J774. Eur J Immunol 1998, 28: 1570-1577

54. Shibuya K, Abe T, and Fujita T: Decay-accelerating factor functions as a signal transducing molecule for human monocytes. J Immunol 1992, 149: 1758-1762

55. Shenoy-Scaria AM, Kwong J, Fujita T, Olszowy MW, Shaw AS, and Lublin DM: Signal transduction through decay-accelerating factor. Interaction of glycosyl-phosphatidylinositol anchor and protein tyrosine kinases p56lck and p59fyn 1. J Immunol 1992, 149: 3535-3541

56. Kuraya M and Fujita T: Signal transduction via a protein associated with a glycosylphosphatidylinositol-anchored protein, decay-accelerating factor (DAF/CD55). Int Immunol 1998, 10: 473-480

57. Liu J, Miwa T, Hilliard B, Chen Y, Lambris JD, Wells AD, and Song WC: The complement inhibitory protein DAF (CD55) suppresses T cell immunity in vivo. J Exp Med 2005, 201: 567-577

58. Heeger PS, Lalli PN, Lin F, Valujskikh A, Liu J, Muqim N, Xu Y, and Medof ME: Decay-accelerating factor modulates induction of T cell immunity. J Exp Med 2005, 201: 1523-1530

59. Lawrence DW, Bruyninckx WJ, Louis NA, Lublin DM, Stahl GL, Parkos CA, and Colgan SP: Antiadhesive role of apical decay-accelerating factor (CD55) in human neutrophil transmigration across mucosal epithelia. J Exp Med 2003, 198: 999-1010

60. Oksjoki R, Jarva H, Kovanen PT, Laine P, Meri S, and Pentikainen MO: Association between complement factor H and proteoglycans in early human coronary atherosclerotic lesions: implications for local regulation of complement activation. Arterioscler Thromb Vasc Biol 2003, 23: 630-636

61. Kim YU, Kinoshita T, Molina H, Hourcade D, Seya T, Wagner LM, and Holers VM: Mouse complement regulatory protein Crry/p65 uses the specific mechanisms of both human decay-accelerating factor and membrane cofactor protein. J Exp Med 1995, 181: 151-159

62. Shagdarsuren E, Bidzhekov K, Talab YD, Liehn EA, Hristov M, Matthijsen RA, Buurman WA, Zernecke A, and Weber C: C1-Esterase Inhibitor Protects Against Neointima Formation After Arterial Injury in Atherosclerosis-Prone Mice. Circulation 2008, 117: 70-78

63. Torzewski J, Bowyer DE, Waltenberger J, and Fitzsimmons C: Processes in atherogenesis: complement activation. Atherosclerosis 1997, 132: 131-138

64. Seifert PS and Hansson GK: Decay-accelerating factor is expressed on vascular smooth muscle cells in human atherosclerotic lesions. J Clin Invest 1989, 84: 597-604

65. Niculescu F, Rus HG, and Vlaicu R: Decay-accelerating factor regulates complement-mediated damage in the human atherosclerotic wall. Immunol Lett 1990, 26: 17-23

TABLE

Body weights and total serum cholesterol and triglycerides in 22 week old *Ldlr*$^{-/-}$ and *daf-1*$^{-/-}$*Ldlr*$^{-/-}$ mice

	***Ldlr*$^{-/-}$**	***daf-1*$^{-/-}$*Ldlr*$^{-/-}$**
	mean ± SEM	mean ±SEM
Low fat diet		
Number	23	22
Final body weight (g)	25.13 ± 0.68	23.90 ± 0.41
Total cholesterol (mmol/l)	9.44 ± 1.58	9.21 ± 2.15
Triglyceride (mmol/l)	1.76 ± 0.54	1.78 ± 0.46
High fat diet		
Number	18	17
Final body weight (g)	25.22 ± 0.73	26.91 ± 0.45
Total cholesterol (mmol/l)	23.04 ± 3.07	21.88 ± 5.33
Triglyceride (mmol/l)	3.26 ± 0.73	3.36 ± 0.55

FIGURE LEGENDS

Figure 1. DAF deficiency accelerates aortic lipid deposition**: (A-D)** 22 weeks old mice fed a low fat **(A,B)** or a high fat **(C,D)** diet from the age of 12 weeks. Mice were perfused *in vivo* with Sudan IV, after which aortae were excised and processed for *en face* staining as described in Methods. **(A,C)** *Ldlr*$^{-/-}$, **(B,D)** *daf-1*$^{-/-}$*Ldlr*$^{-/-}$. Scale bar represents 1cm; **(E)** Comparison of lesion areas following image analysis of *en face* staining. Values are group means ± SEM**.**

Figure 2: DAF deficiency accelerates atherosclerotic lesion development in the aortic root**: (A-D)** photomicrographs of aortic roots in 22 weeks old mice stained with Oil Red O and counterstained with haematoxylin following **(A,B)** low fat diet or **(C,D)** high fat diet from aged 12 weeks. **(A, C)** *Ldlr*$^{-/-}$, **(B,D)** *daf-1*$^{-/-}$*Ldlr*$^{-/-}$. Scale bars represent 1 mm; **(E)** Comparison of lesion areas in *Ldlr*$^{-/-}$ and *daf-1*$^{-/-}$*Ldlr*$^{-/-}$mice, expressed as a percentage fraction of the aortic root area. Values are group means ± SEM**.**

Figure 3. Increased alpha-actin staining reveals increased lesion complexity in *Daf* $^{-/-}$ *Ldlr* $^{-/-}$ mice fed a low fat diet**:** The photomicrographs are representative section images of aortic root lesions from **(A,C)** *Ldlr*$^{-/-}$ and **(B,D)** *daf-1*$^{-/-}$*Ldlr*$^{-/-}$ mice fed **(A,B)** a low fat or **(C,D)** high fat diet, with VSMC stained with Cy3-conjugated anti-alpha actin (red). Nuclei are stained with TOPRO (far red and near infra-red original, blue pseudocoloured for visualisation). L = lumen; Scale bars represent 50mm. Quantification of **(E)** alpha actin staining and **(F)** macrophages identified by mAb MOMA-2, both expressed as percentage of lesional cells. The histogram shows a

significant increase in VSMC in DAF deficient mice fed a low fat diet. Values are group means ± SEM.

Figure 4. Confocal microscopy showing localization of DAF in relation to endothelial cells, macrophages and VSMC**:** Aortic root sections from high fat-fed *Ldlr*$^{-/-}$ mice were analysed by confocal microscopy to detect the presence of DAF on endothelial cells, macrophages and VSMC. **(A)** Rat anti-mouse DAF (clone MD1), followed by biotinylated polyclonal rabbit anti-rat secondary and development with AlexaFluor® 568-conjugated streptavidin (pseudocoloured green), filled green arrowhead shows strong DAF expression in non-lesional area, whereas open green arrowhead shows weak DAF expression in lesional area; **(B)** AlexaFluor® 488-conjugated anti-CD31 reacting with endothelial cells (pseudocoloured red), filled red arrowhead shows maintained CD31 staining over lesion; **(C)** TOPRO-3 nuclear dye (pseudocoloured blue) and **(D)** merged image of (A), (B) and (C) where filled yellow arrowhead points to colocalisation of CD31 and DAF over non-lesional area (yellow overlay = red/green combined), and open red arrowhead points to positive CD31 (red) but weak DAF (green) expression over lesion; **(E)** rat anti-mouse DAF (clone MD1), followed by biotinylated polyclonal rabbit anti-rat secondary and development with AlexaFluor® 488-conjugated streptavidin (green), filled green arrows point to DAF expression in plaque and in adventitia; **(F)** AlexaFluor® 568-labelled anti-CD68 (macrophages, red), with filled red arrows showing CD68 expression by plaque and adventitia macrophages; **(G)** TOPRO-3 as in (C); **(H)** merged image of (E), (F) and (G), where filled yellow arrows point to colocalisation of CD68 and DAF in some macrophages (yellow = red / green combined), both in the superficial plaque and in adventitia; **(I)** DAF staining as in (E), filled green arrowheads show DAF expression

in intima and adventitia **(J)** Cy3-conjugated anti-alpha actin to identify VSMC (red); **(K)** TOPRO-3 as in (C), and **(L)** merged image of (I), (J) and (K), where open block arrow shows little DAF colocalization with VSMC (if present, would be yellow = red/green combined). Scale bars represent 50µm. L= lumen.

Figure 5. Validation of polyclonal anti-C3d antibody for detecting activated C3**: (A)** ELISAs to detect C3 and C3d in sera from wild-type mice, factor I-deficient mice and sera from wild-type mice incubated with trypsin *in vitro.* Y axis represents optical density (OD) readings. The result is representative of two experiments; **(B-E)** Using a polyclonal anti-C3 antibody, mesangial C3 staining is readily evident in the glomeruli of kidney sections from factor I-deficient mice **(B)**. No staining is seen when an anti-C3d antibody is used **(C)** demonstrating that the anti-C3d antibody does not react with C3 in tissue. Following incubation of the sections with a source of murine factor I, mesangial C3 reactivity becomes apparent using both the anti-C3 **(D)** and anti-C3d antibody **(E)**.

Figure 6. DAF deficiency significantly increases C3d deposition in atherosclerotic lesions**:** Histograms showing percentage of lesion positive for C3 **(A)** and C3d **(C)**, and intensity of positive C3 **(B)** and C3d **(D)** staining, where values are means ± SEM; **(E-J)** Photomicrographs of aortic root lesions of *Ldlr*$^{-/-}$ (**E,G**) and *daf-1*$^{-/-}$*Ldlr*$^{-/-}$ (**F,H**) following a low fat **(E, F)** or high fat **(G,H)** diet were stained for confocal microscopy to visualise C3d; **(I,J)** corresponding IgG controls on section of low fat **(I)** and high fat **(J)** diet fed mouse; **(K,L)** show absence of anti-C3d staining of aortic root sections of 22 week old low fat **(K)** and high fat **(L)** diet high fed C3 deficient *Ldlr*$^{-/-}$ mice. Numbers studied were 16 *Ldlr*$^{-/-}$ and 11 *daf-1*$^{-/-}$*Ldlr*$^{-/-}$ on low fat, and 15 *Ldlr*$^{-/-}$ and 8 *daf-1*$^{-/-}$*Ldlr*$^{-/-}$ on high fat. Scale bars = 50µm.

Figure 7. DAF deficiency significantly increases C5b-9 deposition in atherosclerotic lesions**:** Representatives photomicrographs of aortic root sections of **(A)** a low fat fed *Ldlr*$^{-/-}$ mouse stained with control rabbit IgG (score 0), **(B)** a low fat fed *Ldlr*$^{-/-}$ mouse (score +) stained with anti-C5b-9, and **(C)** a low fat fed *daf-1*$^{-/-}$*Ldlr*$^{-/-}$ mouse (score +++) stained with anti-C5b-9 (score +++). Scale bars represent 100µm; L = lumen. **(D)** shows a the summary of semiquantitative scoring. Statistical analysis was performed with Mann-Whitney test.

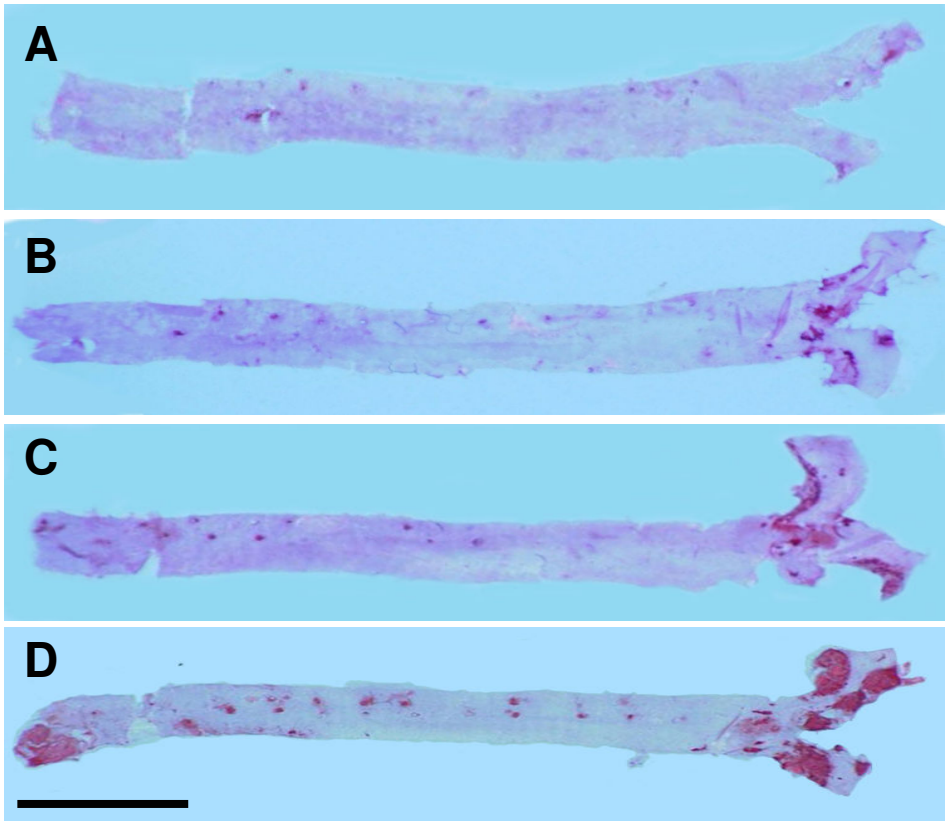
A
B
C
D

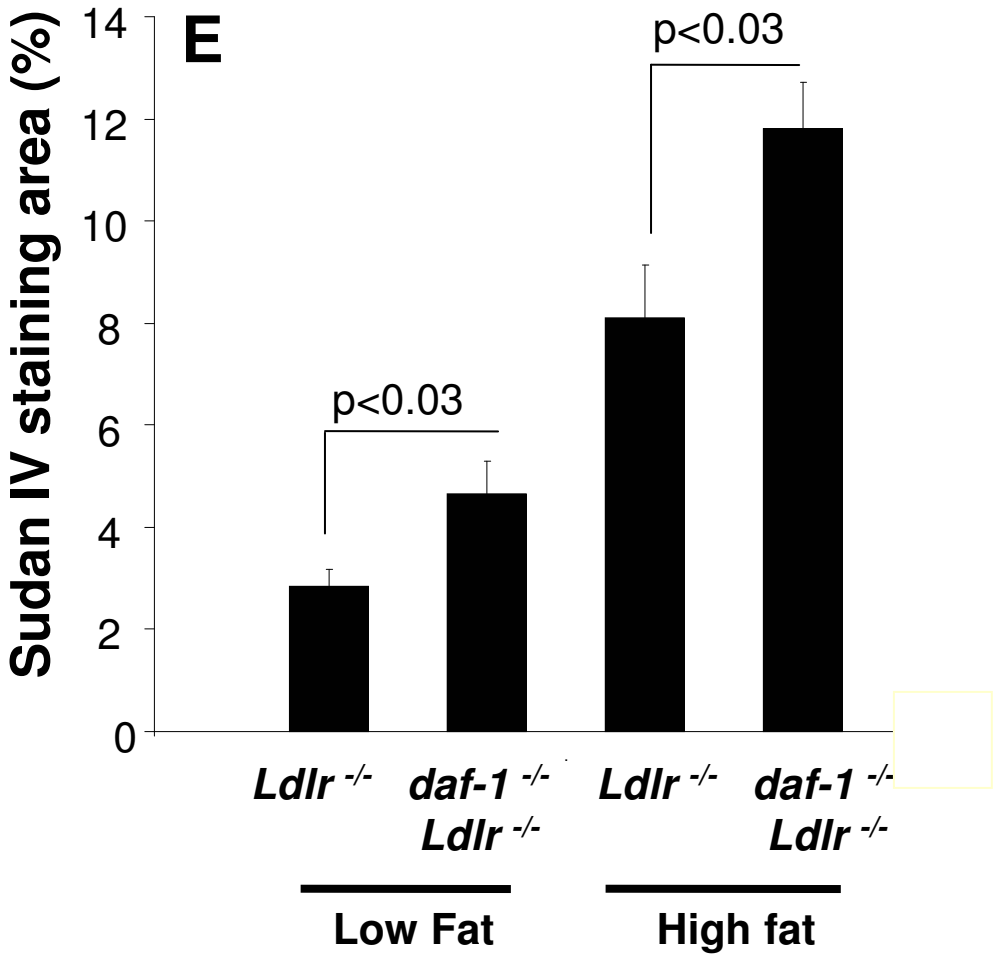
E
Sudan IV staining area (%)
14
12
10
8
6
4
2
0
p<0.03
p<0.03
Ldlr -/-
daf-1 -/- Ldlr -/-
Ldlr -/-
daf-1 -/- Ldlr -/-
Low Fat
High fat

Figure 1

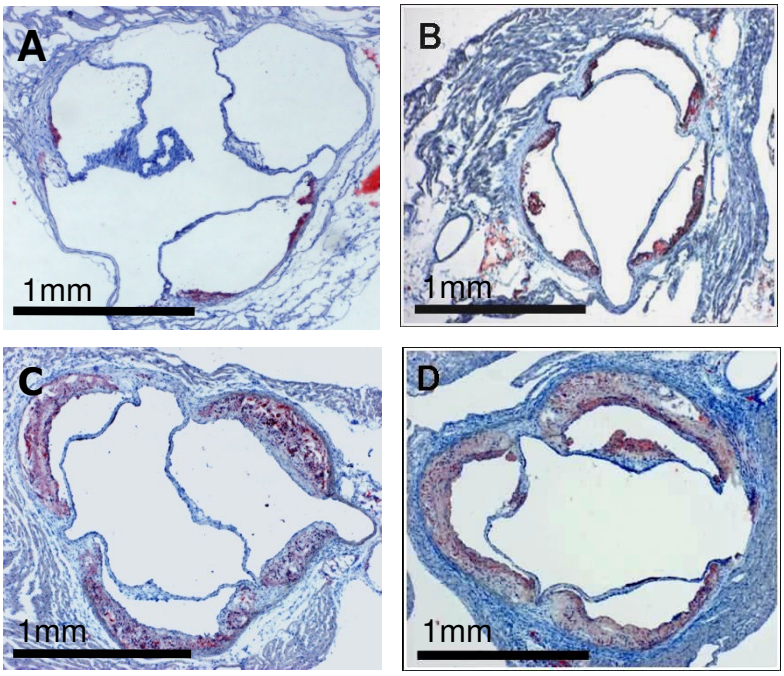
A
1mm
B
1mm
C
1mm
D
1mm

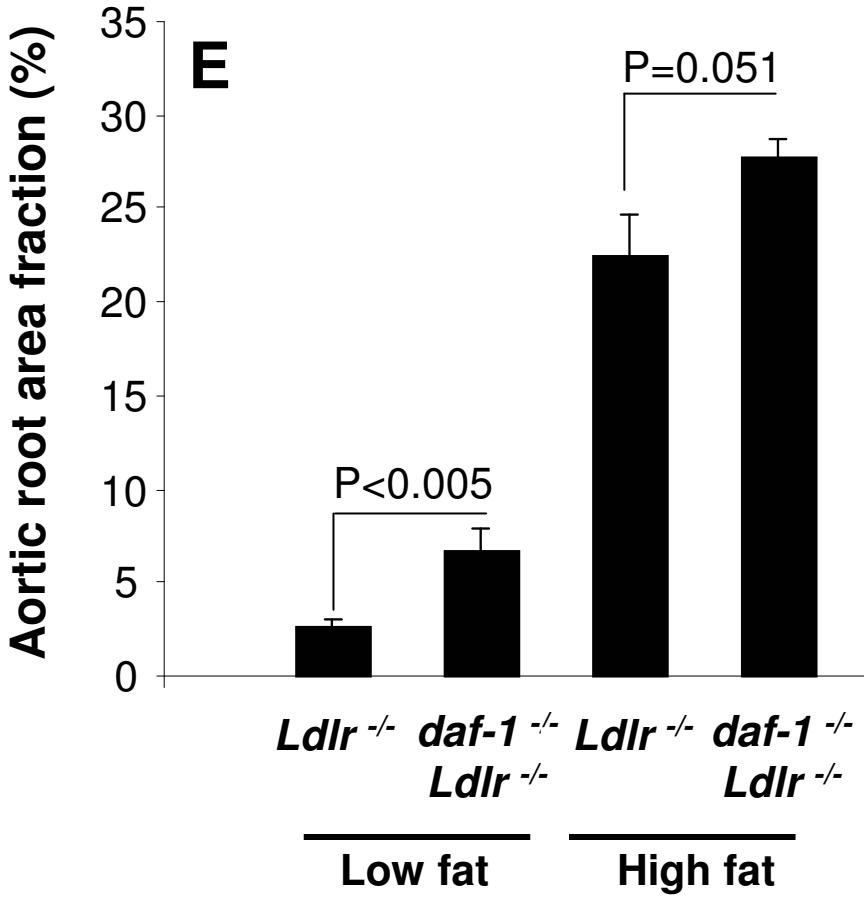
E
Aortic root area fraction (%)
35
30
25
20
15
10
5
0
P<0.005
P=0.051
Ldlr -/-
daf-1 -/- Ldlr -/-
Ldlr -/-
daf-1 -/- Ldlr -/-
Low fat
High fat

Figure 2

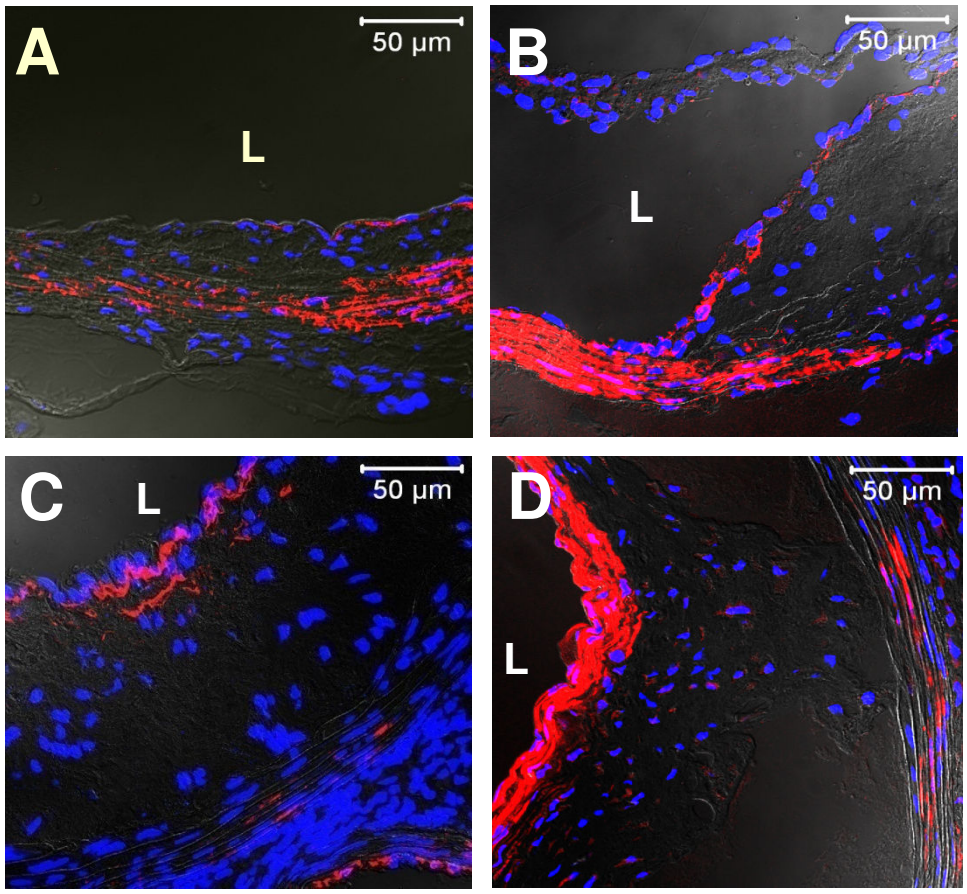
A
50 µm
L
B
50 µm
L
C
L
50 µm
D
50 µm
L

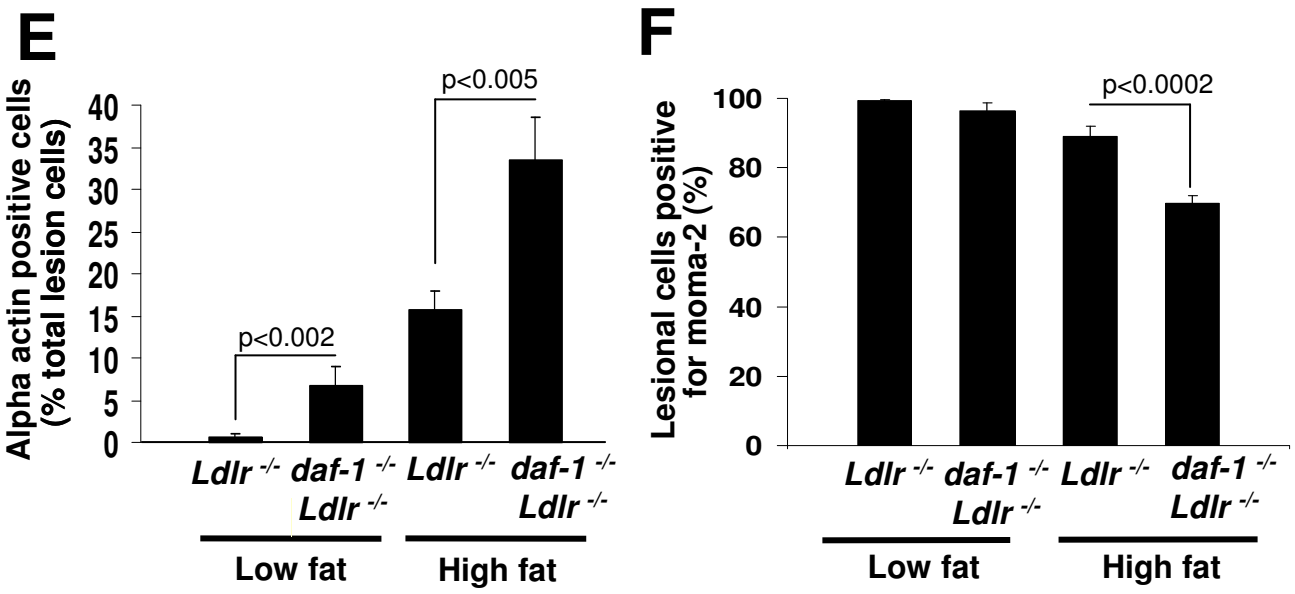
E
Alpha actin positive cells
(% total lesion cells)
40
35
30
25
20
15
10
5
0
p<0.002
p<0.005
Ldlr -/-
daf-1 -/- Ldlr -/-
Ldlr -/-
daf-1 -/- Ldlr -/-
Low fat
High fat
F
Lesional cells positive
for moma-2 (%)
100
80
60
40
20
0
p<0.0002
Ldlr -/-
daf-1 -/- Ldlr -/-
Ldlr -/-
daf-1 -/- Ldlr -/-
Low fat
High fat

Figure 3

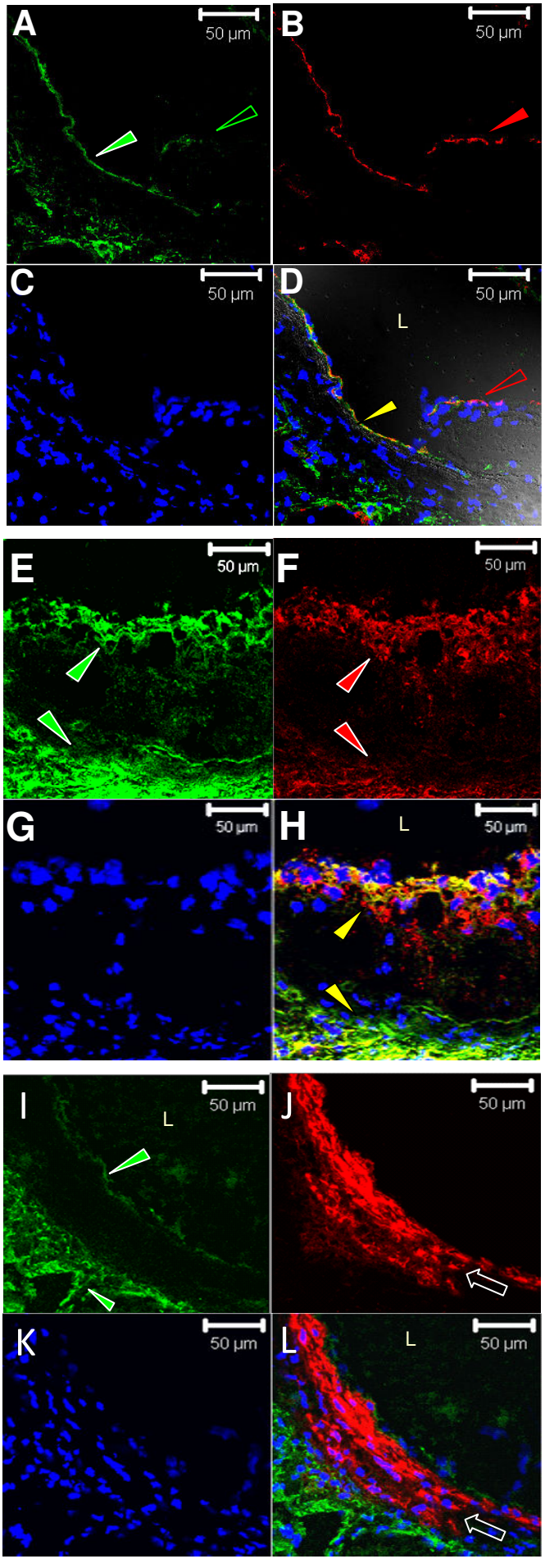
A
50 µm
B
50 µm
C
50 µm
D
50 µm
L
DAF
CD31
E
50 µm
F
50 µm
G
50 µm
H
L
50 µm
DAF
CD68
I
L
50 µm
J
50 µm
K
50 µm
L
L
50 µm
DAF
actin

Figure 4

A

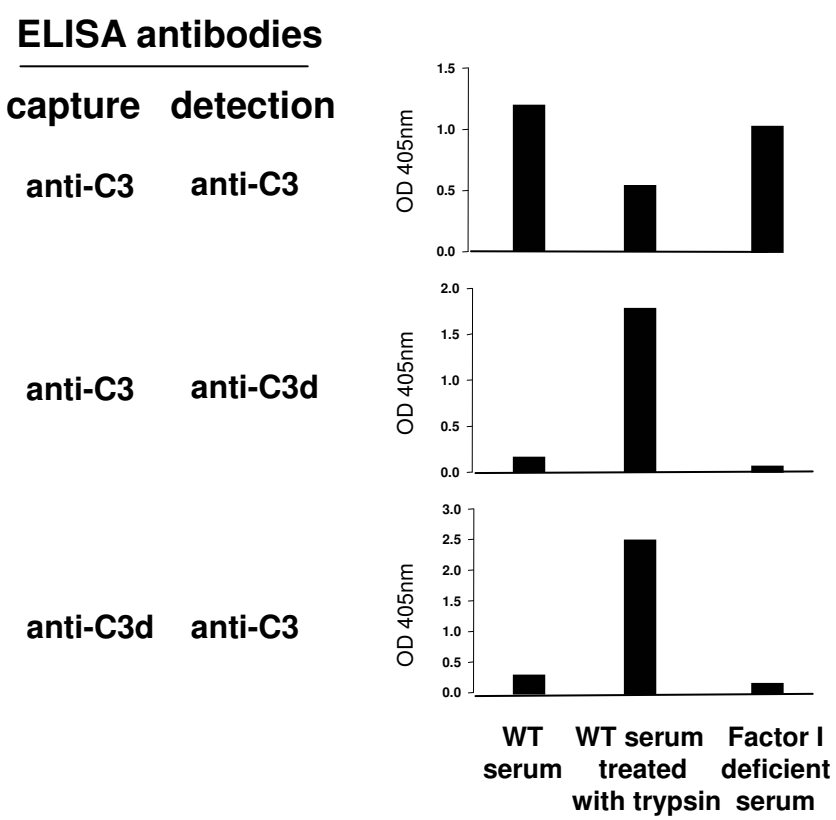
ELISA antibodies
capture
detection
anti-C3
anti-C3
anti-C3
anti-C3d
anti-C3d
anti-C3
OD 405nm
1.5
1.0
0.5
0.0
2.0
1.5
1.0
0.5
0.0
3.0
2.5
2.0
1.5
1.0
0.5
0.0
WT serum
WT serum treated with trypsin
Factor I deficient serum

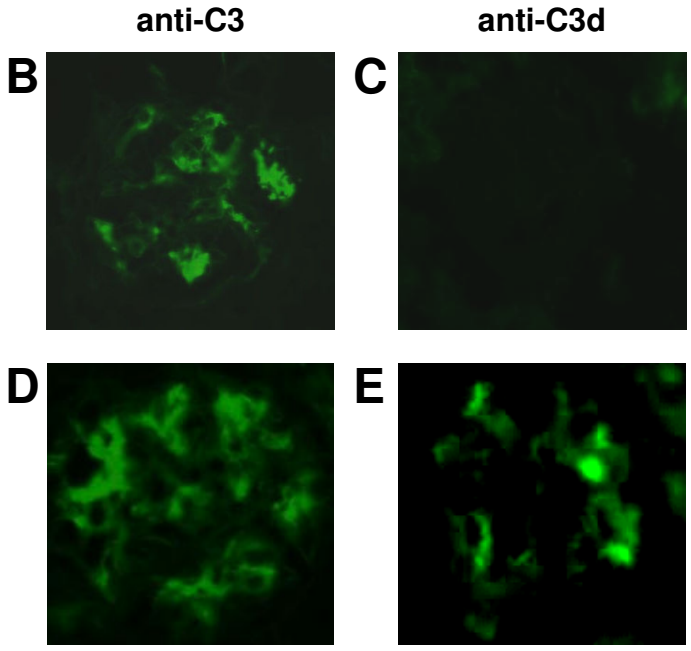
anti-C3
anti-C3d
B
C
D
E

Figure 5

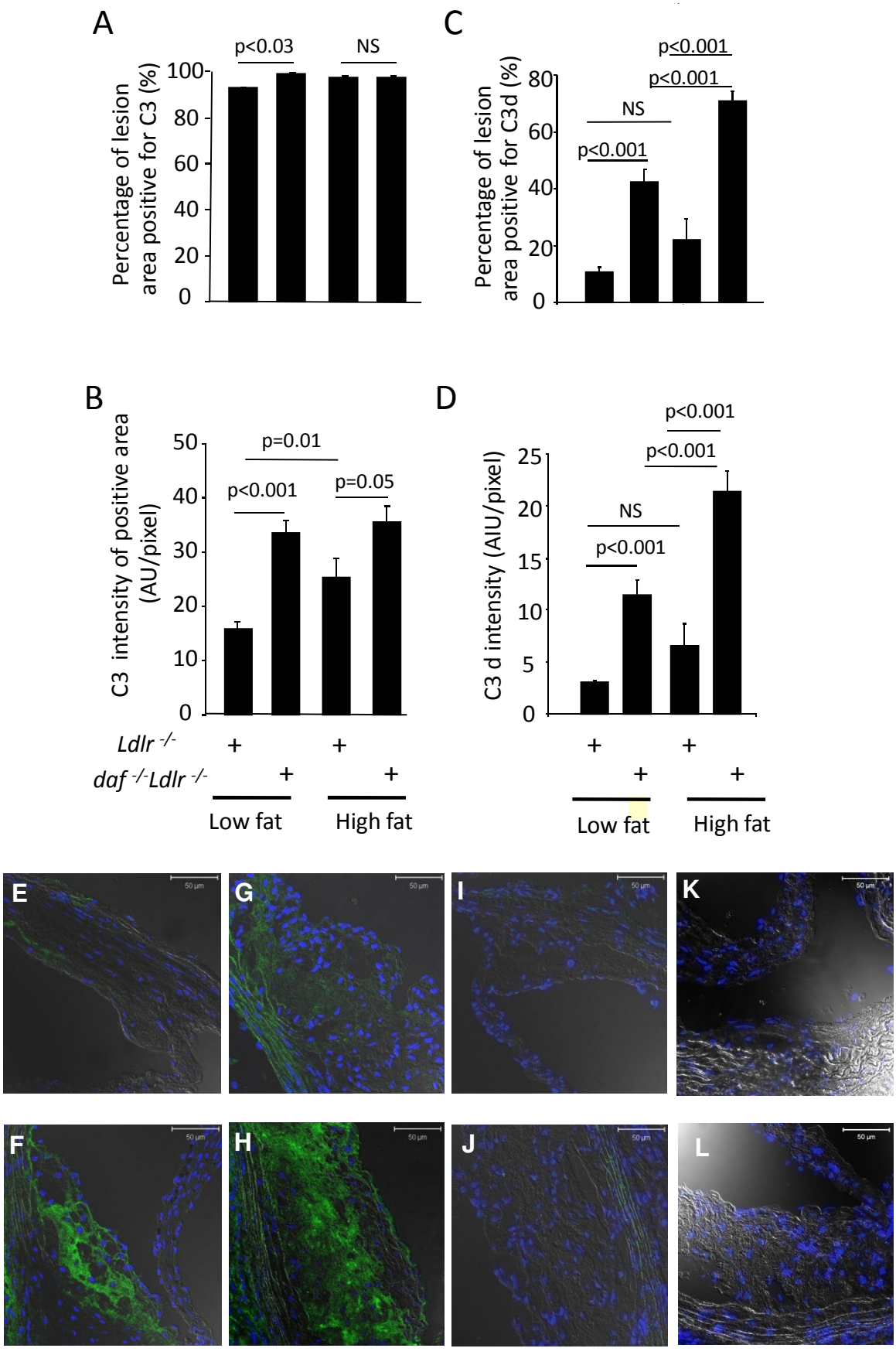
A
p<0.03
NS
Percentage of lesion area positive for C3 (%)
100
80
60
40
20
0
C
p<0.001
p<0.001
NS
p<0.001
Percentage of lesion area positive for C3d (%)
80
60
40
20
0
B
p=0.01
p<0.001
p=0.05
C3 intensity of positive area (AU/pixel)
50
40
30
20
10
0
Ldlr -/-
daf -/-Ldlr -/-
+
+
+
+
Low fat
High fat
D
p<0.001
p<0.001
NS
p<0.001
C3 d intensity (AIU/pixel)
25
20
15
10
5
0
+
+
+
+
Low fat
High fat
E
G
I
K
F
H
J
L
50 µm

Figure 6

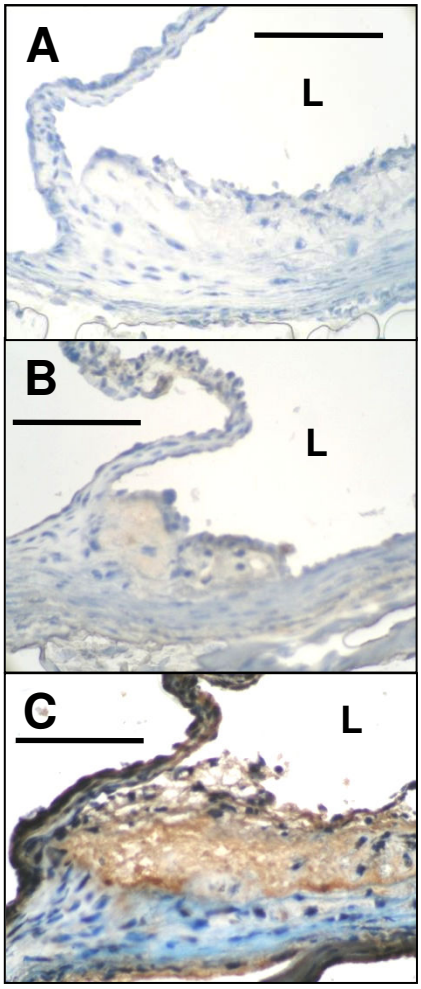
A
L
B
L
C
L

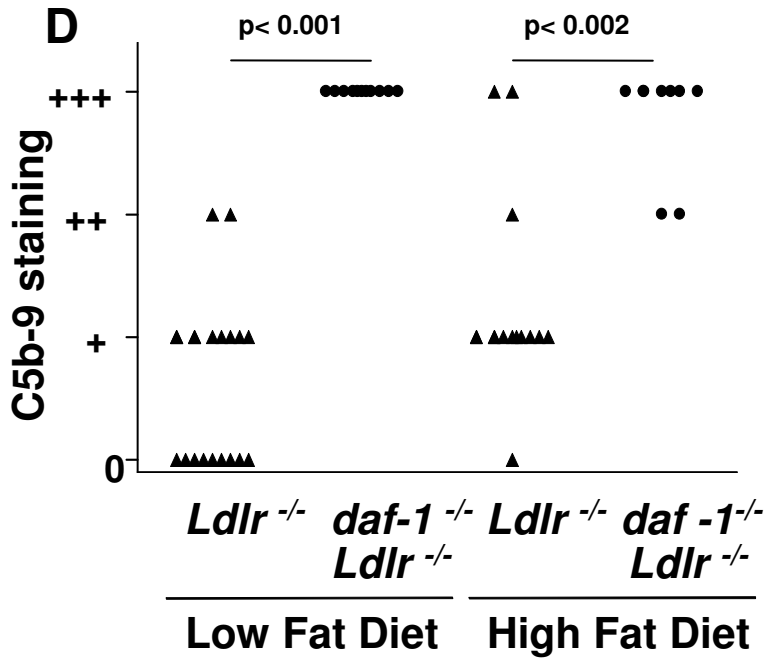
D
p< 0.001
p< 0.002
C5b-9 staining
+++
++
+
0
Ldlr -/-
daf-1 -/- Ldlr -/-
Ldlr -/-
daf -1-/- Ldlr -/-
Low Fat Diet
High Fat Diet

Figure 7